ELSEVIER

Applied Surface Science 150 (1999) 171–177

applied surface science

www.elsevier.nl/locate/apsusc

Pulsed laser ablation of $La_{0.5}Sr_{0.5}CoO_3$

Edward A.F. Span *, Frank J.G. Roesthuis, Dave H.A. Blank, Horst Rogalla

Department of Applied Physics, University of Twente, P.O. Box 217, 7500 AE Enschede, Netherlands

Received 10 February 1999; accepted 28 April 1999

Abstract

The ablation process of $La_{0.5}Sr_{0.5}CoO_3$ by a spatial uniform 248 nm excimer laser beam has been characterized. Ablation rates, changes in the target surface morphology and composition have been studied as a function of the laser fluence. The dependence of the ablation rate on the laser fluence has been explained by a model based on plasma absorption. The threshold fluence for complete dissociation of the surface has been determined and is found equal to 0.7 J/cm^2. Above this threshold, a steady-state target surface condition is obtained within 30 pulses. Below the threshold fluence, CoO nuclei form, which have a pronounced effect on the target composition and morphology. In addition, ellipsometric and reflectance spectra have been measured in the photon energy range of 1.8 to 5.0 eV.

Keywords: $La_{0.5}Sr_{0.5}CoO_3$; Laser ablation; Threshold fluence

1. Introduction

The strontium substituted lanthanum cobaltate $La_{0.5}Sr_{0.5}CoO_3$ (LSCO) is a pseudo-cubic perovskite with a high electronic, thermal and oxygen-ionic conductivity. It also exhibits a good chemical stability and high catalytic activity. LSCO has, therefore, potential application as oxygen separation membrane, electrode material for solid oxide fuel cells, oxidation catalyst and gas sensor material [1–3].

Although material properties of bulk LSCO have been studied extensively for decades, research on the properties and use of LSCO thin films is of recent date. STM studies on LSCO thin films deposited on $SrTiO_3$ and MgO have revealed that LSCO exhibits an isotropic (stepedge) growth mechanism [4]. Consequently, under optimal growth conditions, thin films of LSCO are exceptionally smooth without any type of surface features such as particulates or outgrowths [4–6]. The smooth surface morphology, high electrical conductivity, good chemical stability, plus the fact that LSCO is lattice-matched with many ferroelectric perovskites such as $Pb(Zr,Ti)O_3$ as well as with some high-T_c superconductors like $YBa_2Cu_3O_{7-\delta}$, make LSCO especially attractive for application in, both, ferroelectric and superconducting thin film devices. It has already been demonstrated that ferroelectric capacitors using LSCO electrodes have superior characteristics compared to capacitors using Pt electrodes [7,8]. Besides, it is a promising barrier material for SNS-Josephson junctions [9]. Moreover, $(La,Sr)CoO_3$ thin films are studied for application in thin film fuel cells [10] and thin film oxygen separation membranes [11].

Because of its simplicity and versatility, Pulsed Laser Deposition (PLD) is one of the most suitable methods for fabrication of these thin film devices.

* Corresponding author. Tel.: +31-53-4893126; fax: +31-53-4891099; E-mail: e.a.f.span@tn.utwente.nl

0169-4332/99/$ - see front matter
PII: S0169-4332(99)00242-1

An important issue in PLD of complex oxides is the stoichiometric transference of material from target to substrate. In order to obtain films having the same stoichiometry as the target, a specific threshold fluence has to be exceeded [12–14]. However, only a few complex oxides have been studied with respect to the laser–target interaction during PLD. Dam et al. [15] performed detailed studies on the ablation mechanism of $YBa_2Cu_3O_{7-\delta}$, Y_2BaCuO_5 and $SrTiO_3$ and identified two different mechanisms for non-stoichiometric ablation below the threshold fluence. In the Y–Ba–Cu–O system, ablation below the stoichiometry threshold (1.0 J/cm^2 for the 123-phase and 1.2 J/cm^2 for the 211-phase) results in the formation of the stable Y_2O_3 phase due to incongruent melting of these materials. In congruently melting materials, on the other hand, ablation below the stoichiometry threshold (1.3 J/cm^2 for $SrTiO_3$) results in non-stoichiometric films due to preferential ablation of one of the constituents [16].

In this paper, we characterize the erosion of the LSCO target due to the pulsed laser ablation process, using a well-defined uniform laser spot. The ablation depth per pulse is measured and compared to a model based on the plasma absorption coefficient. In order to determine the laser ablation threshold we studied changes in the target surface morphology and stoichiometry as a function of fluence and the number of pulses. In addition, we measured the optical properties of the target and calculated the reflectivity and optical absorption.

2. Experimental

The laser ablation is carried out in a vacuum chamber with a background pressure of 10^{-4} mbar. A pulsed 248 nm, 30 ns KrF excimer laser beam (Lambda Physik) enters the vacuum chamber at an angle of 45° with respect to the target. A very small, homogenous and rectangular part of the laser beam is projected on the target by means of projection optics consisting of a mask, mirror and a lens with a focal length of $f = 454$ mm. The spatial energy variation within this laser spot is about 5%. By varying the position of the mask and lens according to the lens formula, the demagnification of the spot area on the target can be varied, taking into account a factor $2^{-1/2}$ for the 45° angle of incidence on the target. After ablation, the size of the impact area of the laser beam on the target is verified by measuring the widths of the obtained ablation crater. The energy at the target is determined by measuring the spot energy with an energy meter, corrected for the total energy loss (28%) in the mirror, lens and vacuum chamber window. By varying, both, the laser energy and the spot size on the target, the energy density (fluence) at the target can be varied from 0.2 to 3 J/cm^2. In all experiments, the laser repetition frequency is kept constant at 5 Hz.

The ablation rate from the stationary stoichiometric LSCO target (polycrystalline, 99% dense) is determined by scanning the obtained crater depths with a Tencor profilometer. In order to obtain crater depths of several micrometers for each fluence, we varied the number of pulses from 100 for high fluences to 1000 for very low fluences. Changes in the target morphology after ablation are investigated by SEM and changes in the surface composition of the target are determined by Energy Dispersive X-ray analysis (EDX), using 15 keV primary electrons and averaging over an area of 60×60 μm. Optical data were obtained using a (rotating-polarizer) spectroscopic ellipsometer, in an energy window of 1.8 to 5.0 eV (689 to 248 nm). The optical parameters measured were converted to the complex dielectric function $\tilde{\varepsilon}$ using the two-phase model [17].

3. Results and discussion

3.1. Ablation rates

Fig. 1 shows the crater depth in the LSCO target after 200 pulses with an energy density of 0.8 J/cm^2. Small brims are visible on the edges due to redeposition of ablated material against the sidewalls of the crater. The uniform erosion also evidences the uniformity of the laser spot. Fig. 2 shows the measured variation of the ablation depth per pulse with fluence. At a fluence of 0.2 J/cm^2 a very small plume is generated by the ablated target material. Since this plume was sometimes absent due to the relative large energy fluctuations ($\pm 10\%$) caused by instability of the laser at very low energies, we estimate that the threshold fluence for ablation is about 0.18 J/cm^2. The ablation rate just above this threshold is less than 0.1 nm/pulse. In the range of 0.3 to 3 J/cm^2, a

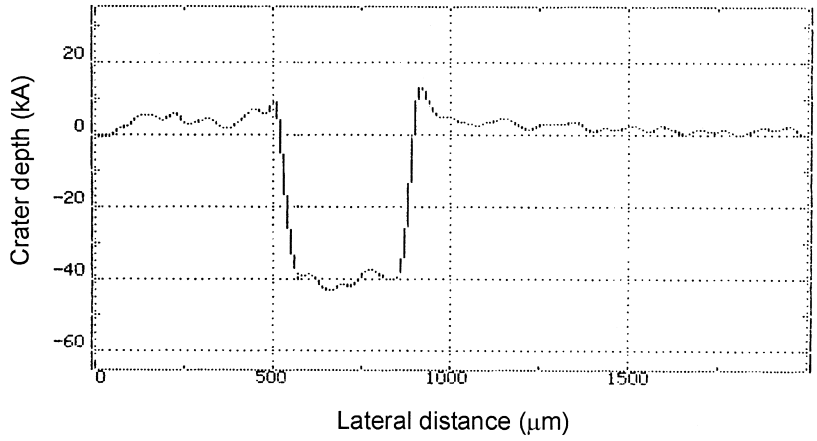

Fig. 1. Cross-section of the ablation crater in the LSCO target resulting from 200 laser pulses with a fluence of 0.8 J/cm^2.

strong increase in ablation rate is observed, up to more than 50 nm per pulse.

For metallic solids as LSCO, a linear increase in the evaporated thickness of the target is expected above the ablation threshold according to [18]:

$$\Delta x = (1 - R)(E - E_{\text{th}})/\Delta H \qquad (1)$$

where Δx represents the amount of ablated material per pulse, R the reflection coefficient, E the energy density (fluence) and ΔH the enthalpy of dissociation. In this model, the threshold fluence E_{th}, which represents energy losses due to heat conduction and plasma absorption, is assumed to be independent of E. Fig. 2 shows an initial linear increase in the evaporated thickness Δx with increasing fluence for low fluences. However, this linear relationship does not hold for higher fluences. This is explained by a strong increase in plasma absorption at higher ablation rates. Absorption of incident laser energy by the plasma leads to an increase in the internal energy of the plasma and to a decrease in the net energy that is supplied to the target to cause vaporization.

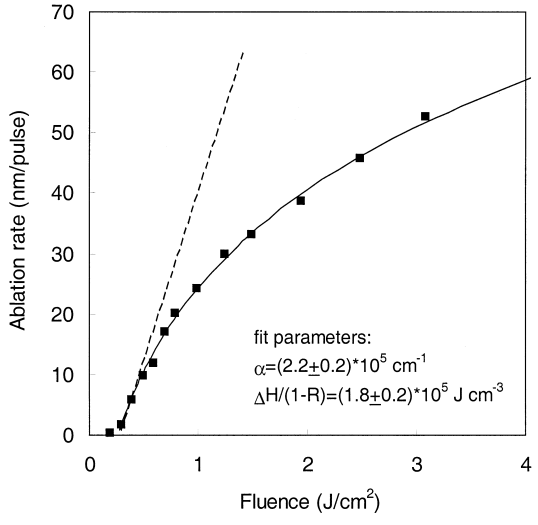

Fig. 2. Experimental and calculated ablation depth of LSCO as a function of laser fluence. The dashed line represents the calculated ablation rate with constant plasma absorption.

The amount of laser energy that is absorbed by the plasma depends on the plasma absorption coefficient α_{p} and the dimension of the plasma in the direction of the incident laser beam d_{p}. However, the parameters that determine α_{p} (like electron density and plasma temperature) just as the plasma dimensions are strongly time-dependent and are, therefore, difficult to estimate. By introducing the concept of the simulated plasma absorption coefficient α_{simul} [19], the time dependence of both d_{p} and the parameters that control α_{p} need not to be known. The simulated plasma absorption coefficient α_{simul} is assumed to be a time-independent constant, whereas the evaporated thickness Δx is a measure for the plasma dimension. The amount of incident laser intensity that is absorbed by the plasma P_{plasma} can thus be written as:

$$P_{\text{plasma}} = P_{\text{inc}} - P_{\text{net}} = P_{\text{inc}}\left(1 - \exp\left(-\alpha_{\text{p}} d_{\text{p}}\right)\right)$$
$$= P_{\text{inc}}\left(1 - \exp\left(-\alpha_{\text{simul}} \Delta x\right)\right) \qquad (2)$$

where P_{inc} and P_{net} are the total incident laser power density (which is proportional to the fluence) and the net laser power density that is supplied to the target, respectively. By combining Eqs. (1) and (2) a model is obtained which relates Δx to the fluence, with α_{simul} and $\Delta H/(1-R)$ as unknown parameters. We checked the validity of this model by comparing simulated curves with our experimental ablation rates. It was found that the experimental and simulated curves could be matched by choosing appropriate values for α_{simul} and $\Delta H/(1-R)$. By performing a least squares fitting procedure, we found a value of $(2.2 \pm 0.2) \times 10^5$ cm^{-1} and $(1.8 \pm 0.2) \times 10^5$ J/cm^3 for α_{simul} and $\Delta H/(1-R)$, respectively. Values of α_{simul} that have been reported for $YBa_2Cu_3O_{7-\delta}$ vary, depending on the type of excimer laser used, from 2.3 to 6.0×10^5 cm^{-1} [19]. Our model also implies an ablation threshold of 0.26 J/cm^2, which is somewhat larger than the observed ablation threshold. We attribute this difference to the influence of the surface morphology that develops in the range of 0.3 to 0.4 J/cm^2. This surface morphology, which will be discussed below, leads to lower overall ablation rates due to redeposition of ablation debris. Consequently, the fit will give a somewhat larger ablation threshold.

3.2. Morphology and composition

SEM studies of the target after ablation reveal a drastic change in the surface morphology as a function of fluence (Fig. 3). For fluences larger than 0.7 J/cm^2, the surface of the LSCO target is relatively

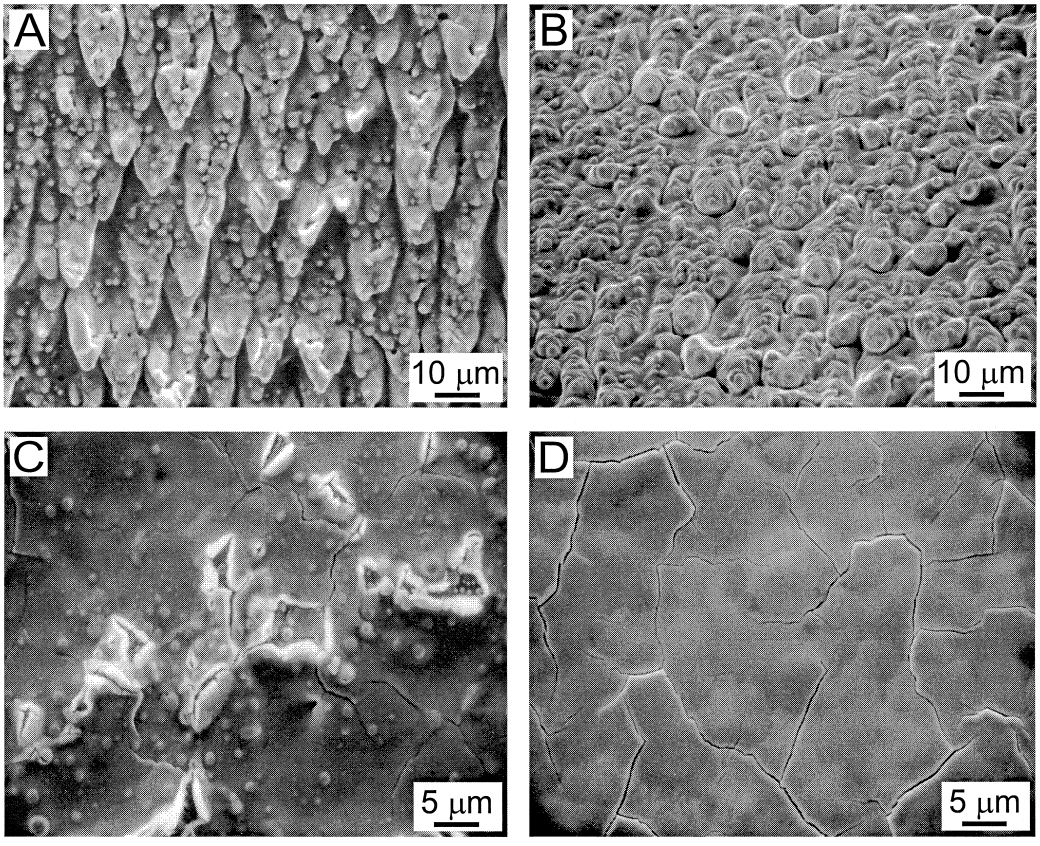

Fig. 3. Laser-induced target morphology of LSCO after 1000 laser pulses at fluences of 0.4 J/cm^2 (a) and (b), 0.5 J/cm^2 (c) and for fluences $\geq$ 0.7 J/cm^2 (d). In (a), (c) and (d) the SEM picture is taken normal to the target surface. The pillars in (a) point towards the incoming laser beam. In (b) the SEM picture is taken at an angle of 45° to the surface normal, along the incoming laser beam.

smooth with many subsurface cracks due to surface melting and subsequent fast recrystallization (quenching) of the liquid phases after ablation. Below a critical fluence of 0.7 J/cm^2, the changes in the target morphology become very sensitive to the fluence. At fluences of 0.5 and 0.6 J/cm^2, the cracked subsurface contains many spherical globules of maximal 1 μm in size. After prolonged ablation these globules crack, resulting in blister-like structures with raised borders (Fig. 3c). Lowering the fluence to 0.3–0.4 J/cm^2 leads to the formation of large cones, covered with many boulders and directed along the incoming laser beam (Fig. 3a,b). From EDX, it turned out that the spherical globules as well as the top of the cones consist of pure cobalt.

For fluences larger than 0.7 J/cm^2, very high temperatures will develop at the target surface. Consequently, the surface layer transforms completely into a melt, which upon resolidification, returns into a homogenous surface layer, containing only low-threshold phases. For fluences below 0.7 J/cm^2, phase separation occurs due to lower surface temperatures. The phase separation results in the formation of high-threshold Co containing secondary phase nuclei, embedded in a matrix of LSCO. As we will show below, these Co containing nuclei consist of CoO, since LSCO will undergo a phase transformation during ablation in which CoO is formed. A second mechanism that simultaneously might play a role in the formation of CoO nuclei, is the melting and resolidification behavior of LSCO. Because CoO has a higher melting point than LSCO (viz. 1795 and ~1400°C, respectively), CoO nuclei might crystallize from the melt before the resolidification is completed. In the intermediate fluence range of 0.5 to 0.6 J/cm^2, these CoO nuclei are stable and they will grow into spherical globules. Because these globules are eventually destroyed, they do not have a significant influence on the overall ablation rate and still deep ablation craters are obtained. On the other hand, a fluence of 0.4 J/cm^2 is too low to destroy the CoO globules with the consequence that the LSCO matrix around the globules is ablated, whereas material that is shielded by the globules from the incoming laser beam is not ablated. Consequently, cones with spherical CoO globules on the ends are formed, pointing in the direction of the incoming laser beam.

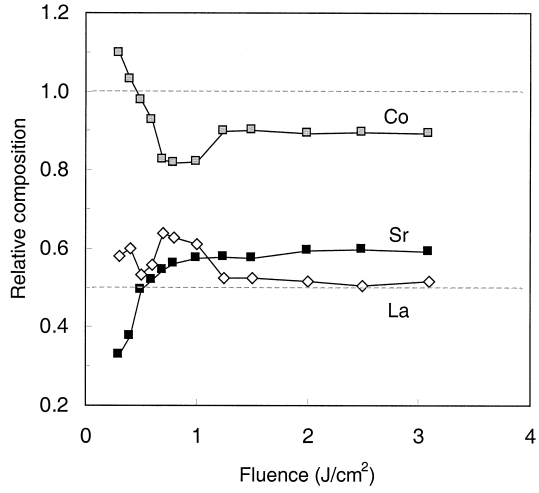

Fig. 4. Relative composition of the LSCO target surface as a function of fluence. The metal composition is normalized to a sum of 2.

Fig. 4 shows the relative composition of the ablation craters as determined by EDX. Investigation of the non-ablated target gave a metal composition that deviated less than 5% from the nominal composition. For fluences larger than 0.7 J/cm^2, a steady-state surface condition is obtained within 30 pulses, as we demonstrate in Fig. 5 for a fluence of 1.5 J/cm^2. Small differences in the steady-state composition between Figs. 4 and 5 are attributed to local variations in the target composition. We also verified that the composition of the ablation craters does not change when oxygen is introduced into the vacuum chamber up to 0.1 mbar. According to Fig. 4, the target surface goes through a compositional transition around ~1.2 J/cm^2. Since this transition is not marked by a morphological change, we conclude that only low-threshold phases are involved in this transition. For higher fluences, an equilibrium composition establishes which is slightly off-stoichiometric. For fluences below 0.7 J/cm^2, we see a strong increase in the relative amount of Co with decreasing fluence, which is consistent with our observation of the formation of refractive CoO nuclei.

By means of a two-probe measurement, we found that, for fluences ≥0.7 J/cm^2, the electrical resistance of the target surface increases 2 to 3 orders of magnitude during the first five laser pulses. After achieving the steady-state condition, the resistance is

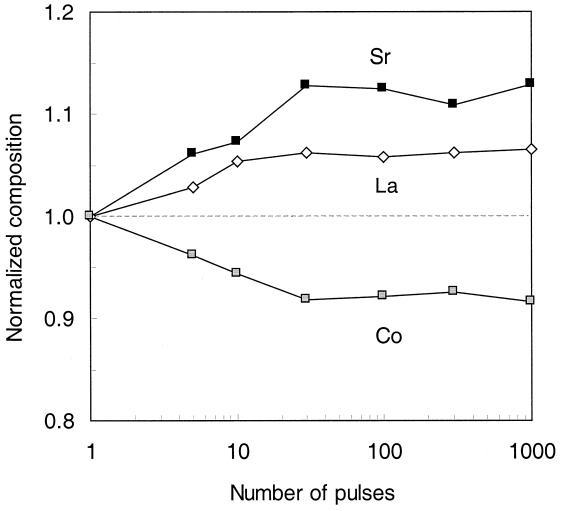

Fig. 5. Change in the LSCO target surface composition as a function of the number of laser pulses for a fluence of 1.5 J/cm^2. Data have been normalized to the composition of the unablated target, which is plotted at the intersection with the *y*-axis.

$\sim 10^4$ times higher compared to the resistance of the non-ablated target. This increase in resistance indicates that immediately an oxygen-deficient surface layer forms since the electrical resistance of LSCO increases many orders of magnitude with decreasing oxygen content [20,21].

It is important to note that we never observed any splashing phenomena, neither on target nor on films, which is in contrast to observations made by Dat et al. [5]. They observed that after prolonged ablation at 1.1 J/cm^2 splashing occurred, which they attributed to a decrease in thermal conductivity consequent on oxygen loss. Because during ablation the electrical conductivity of the target decreases, a decrease in thermal conductivity can also be expected, since the thermal and electrical conductivity of conducting ceramics are related by the Wiedeman–Franz–Lorenz relation [22]. However, we do not believe that this effect can cause splashing in case of LSCO, since a steady-state surface condition is obtained within only 30 pulses. To our opinion, the observed splashing phenomena as observed by Dat et al. might be related to a lower target density and/or inaccurate focusing of the laser beam on the target.

The observation that an off-stoichiometric steady-state surface layer is obtained is related to the observation that upon oxygen removal in the temperature range close to the sintering temperature, $La_{1-x}Sr_xCoO_{3-\delta}$ decomposes according to [23,24]:

$$La_{1-x}Sr_xCoO_{3-\delta} \rightarrow r\,La_{1-x'}Sr_{x'}CoO_{3-\delta'} + w\left(La_{1-y}Sr_y\right)_2CoO_4 + v\,CoO + z\,O_2 \qquad (3)$$

with $r + w + v = 1$. Upon further oxygen removal, also $La_4Co_3O_{10}$ and $SrCoO_x$ can be formed [23].

It is well known from sputter deposition that stoichiometric films can be obtained from compositionally modified target surfaces after reaching steady state, as has been demonstrated by Auciello and Krauss [25] for $YBa_2Cu_3O_{7-\delta}$. In order to verify this for PLD, we investigated the composition of several thick LSCO films, deposited on α-Al_2O_3 substrates, using a fluence of 1.5 J/cm^2. It was found that the atomic composition of these films consisted of (25 ± 3)% La, (25 ± 3)% Sr and (50 ± 1)% Co.

3.3. Optical

In Fig. 6 we present the optical response in the interband transition range of the (polished) LSCO target before ablation, represented by the complex dielectric function $\tilde{\varepsilon}$. We find that an absorption peak is located in the UV-region, just outside the detection window. From the spectra, we calculated

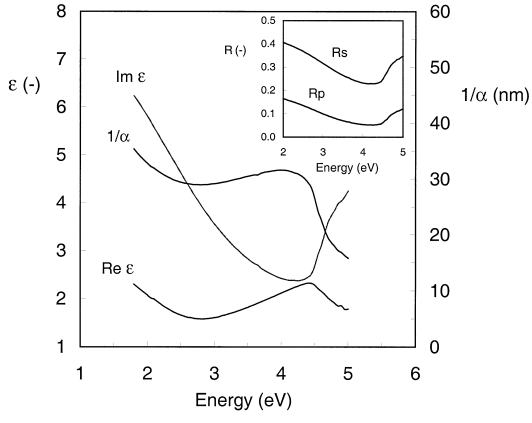

Fig. 6. Complex dielectric function and optical absorption of the LSCO target. The inset shows the reflectance spectra for *p*- and *s*-polarized light incident at an angle of 45°.

the optical absorption depth $1/\alpha$ and the reflectance for light incident at 45°. It is found that the target surface is highly absorbing, as is expected for metallic solids. At the laser wavelength, which corresponds to 5.0 eV, the optical absorption depth of the LSCO target equals 16 nm. At this wavelength, the effective reflectance R for light incident at 45° is 0.26. According to Eq. (1), this would imply that ΔH is about 2.4×10^5 J/cm^3. However, it is expected that the optical response and, consequently, the optical absorption length and reflectance, change during the first laser pulses, since the target surface changes from metallic to insulating. Unfortunately, it was not possible to measure the optical response of the target after ablation due to the too large diffuse reflection from the recrystallized surface after ablation.

4. Conclusions

Fluences above 0.7 J/cm^2 provide enough energy to the LSCO target for complete dissociation of the surface with the consequence that secondary high-threshold phases do not form. In this regime, a steady-state target surface is obtained within 30 pulses. Lowering the fluence leads to the formation of high-threshold phases in the form of CoO nuclei which have a pronounced effect on the target composition and morphology. The dependence of the ablation rate on the fluence has been determined and explained by a model based on plasma absorption. Moreover, the complex dielectric function and reflectance spectra have been measured. For the enthalpy of dissociation, a value of 2.4×10^5 J/cm^3 is found.

Acknowledgements

We would like to thank Natascha Sibelt for the fabrication of the LSCO targets, Mark Smithers for the EDX measurements and Herbert Wormeester for the ellipsometry measurements. This work is financially supported by the Dutch technology foundation STW (Stichting Technische Wetenschappen).

References

[1] Y. Teraoka, H. Zhang, S. Furukawa, N. Yamazoe, Chem. Lett. (1985) 1743.
[2] Y. Kaga, Y. Ohno, K. Tsukamoto, F. Uchiyama, M.J. Lain, T. Nakajima, Solid State Ionics 40–41 (1990) 1000.
[3] T. Nakamura, M. Misono, Y. Yoneda, J. Catal. 83 (1983) 151.
[4] J.T. Cheung, P.E.D. Morgan, D.H. Lowndes, X.-Y. Zheng, J. Breen, Appl. Phys. Lett. 62 (1993) 2045.
[5] R. Dat, O. Auciello, D.J. Lichtenwalner, A.I. Kingon, J. Mater. Res. 11 (1996) 1514.
[6] M. Li, Z.-L. Wang, S. Fan, Q.-T. Zhao, G. Xiong, Thin Solid Films 323 (1998) 304.
[7] R. Ramesh, H. Gilchrist, T. Sands, V.G. Keramidas, R. Haakenaasen, D.K. Fork, Appl. Phys. Lett. 63 (1993) 3592.
[8] R. Ramesh, J. Lee, T. Sands, V.G. Keramidas, O. Auciello, Appl. Phys. Lett. 64 (1994) 2511.
[9] P.W. Chan, W. Wu, K.H. Wong, K.Y. Tong, J.T. Cheung, J. Phys. D: Appl. Phys. 30 (1997) 957.
[10] L.G. Coccia, G.C. Tyrrell, J.A. Kilner, D. Walner, R.J. Chater, I.W. Boyd, Appl. Surf. Sci. 96–98 (1996) 795.
[11] Y. Teraoka, T. Fukuda, N. Miura, N. Yamazoe, J. Ceram. Soc. Jpn. Int. Ed. 97 (1989) 523.
[12] T. Venkatesan, X.D. Wu, A. Inam, J.B. Wachtman, Appl. Phys. Lett. 52 (1988) 1193.
[13] W. Kautek, B. Roas, L. Schultz, Thin Solid Films 191 (1990) 317.
[14] B. Dam, J.H. Rector, M.F. Chang, S. Kars, D.G. de Groot, R. Griessen, Appl. Phys Lett. 65 (1994) 1581.
[15] B. Dam, J.H. Rector, J. Johansson, S. Kars, R. Griessen, Appl. Surf. Sci. 96–98 (1996) 679.
[16] B. Dam, J.H. Rector, J. Johansson, J. Huijbregtse, D.G. de Groot, J. Appl. Phys. 83 (1998) 3386.
[17] D.E. Aspnes, in: B. Seraphin (Ed.), Optical Properties of Solids: New Developments, North-Holland, Amsterdam, 1976, p. 808.
[18] R.K. Singh, O.W. Holland, J. Narayan, J. Appl. Phys. 68 (1990) 233.
[19] R.K. Singh, D. Kumar, Mater. Sci. Eng. R 22 (1998) 113.
[20] S. Madhukar, S. Aggerwal, A.M. Dhote, R. Ramesh, A. Krishnan, D.J. Keeble, E.H. Poindexter, J. Appl. Phys. 81 (1997) 3543.
[21] D.J. Keeble, A. Krishnan, T. Friessnegg, B. Nielsen, S. Madhukar, S. Aggerwal, R. Ramesh, E.H. Poindexter, Appl. Phys. Lett. 73 (1998) 508.
[22] P.E.D. Morgan, J. Am. Ceram. Soc. 58 (1975) 349.
[23] V.A. Cherepanov, L.Y. Barkhatova, A.N. Petrov, V.I. Voronin, Proc. 4th Int. Symp. on Solid Oxide Fuel Cells (SOFC IV), in: M. Dokiya, O. Yamamoto, H. Tagawa, S.C. Singhal (Eds.), ECS Proc. 95-1, 1995, p. 434.
[24] F. Morin, G. Trudel, Y. Denos, Solid State Ionics 96 (1997) 129.
[25] O. Auciello, A.R. Krauss, Am. Inst. Phys., Conf. Proc. 165 (1988) 114.